1969MNRAS.144..485S

Mon. Not. R. astr. Soc. (1969) **144**, 485–510.

CEPHEID PULSATION—II

Models Fitted to Evolutionary Tracks

R. S. Stobie

(Communicated by the Director, Institute of Theoretical Astronomy, Cambridge)

(Received 1968 October 1)

SUMMARY

The results of a survey of classical Cepheids are presented. The masses and luminosities of the models in the survey were chosen to correspond to where the evolutionary tracks of 5–$9M_{\odot}$ stars cross the Cepheid strip. The effect of helium content on the position of the high T_e boundary of the instability strip is examined and it is found that for every 15 per cent increase in helium (by mass) the strip shifts by ~ 600 °K to higher T_e.

Three different modes of pulsation are investigated for instability—fundamental, first and second modes. The existence of second mode instability is confirmed for three stars all of which have a period less than two days.

The presence of secondary bumps in the light and velocity curves was a prominent feature of many of the models. However, in no case did the bump occur (for a given period) at the phase expected from a comparison with observation. The only way in which the phase of the bump can be brought into agreement with observation is for the mass, at a given luminosity, to be reduced by a factor ~ 2 compared to the evolutionary calculations.

1. INTRODUCTION

There is a wealth of observational material on classical Cepheids not only in our own Galaxy but also in external systems. The accumulation of data on their periods, amplitudes, light and velocity curves has led to fairly well established relations between these parameters, e.g. period-amplitude, period-colour and period-phase of bump relations. The phase of the bump here is defined as the time, measured as a fraction of a period by which the maximum luminosity of the bump lags behind the instant when the luminosity curve passes through its static value on the ascending branch. Observationally, this ' static value ' can be calculated by integrating the luminosity curve throughout one complete cycle and then dividing by the period. However, the one relation that is not so well established is the period–absolute magnitude relation and this relation is fundamental to any work involving Cepheids as distance indicators. The principal uncertainty lies in the zero point of this relation of which the best determination, at present, rests solely on the five Cepheids known to exist in galactic clusters. As classical Cepheids in the past have been used principally as distance indicators, it is imperative that the zero point of the period–absolute magnitude relation be established as accurately as possible.

In order to compare the group properties of Cepheids in theory and in observation, we ran a survey covering a range of mass, luminosity, effective temperature and chemical composition. (The technique used to calculate the full amplitude pulsation

Downloaded from https://academic.oup.com/mnras/article/144/4/485/2602797 by guest on 21 August 2022

© Royal Astronomical Society • Provided by the NASA Astrophysics Data System

1969MNRAS.144..485S

of a variable star is described in Paper I of this series.) From this survey we hoped to be able to determine the chemical composition and the mass–luminosity relation of these variables, both of which are essential for deriving the period-luminosity (or period–absolute magnitude) relation. It is also important to know whether or not this relation is constant from one galactic system to another, particularly as there are well known differences between the short period Cepheids in the Small Magellanic Cloud and in the solar neighbourhood.

Observationally, Cepheids exhibit a well defined sequence of secondary bumps in both the luminosity and velocity curves. The phase of the bump decreases as the period increases and coincides with maximum luminosity at a period of approximately 10 days. It was expected that the non-linear calculations could develop similar bumps and comparison with observation would lead to more insight into the nature of these stars.

2. THE SURVEY

The survey of classical Cepheids was specifically designed to determine the mass and chemical composition of these variables and position of the instability strip in the HR diagram. Because of the large number of parameters which can be varied in this survey, e.g. the mass, luminosity, effective temperature, chemical composition and the particular mode of instability, it is advantageous to find some way of restricting this variation. One way is to take well observed Cepheids (Kraft 1961) with a given M_v and $(B-V)$ and then try to fit the mass to give the observed period. This is precisely what Christy (1966c) has done in examining models of δ Cephei and η Aquilae, where the observational parameters for these two stars were taken from Oke (1961a, b). A second possible way is to take models from the evolutionary tracks of Hofmeister (1967) and Iben (1965, 1966a, b, c) and examine their instability. It is this latter method which has been adopted for the main survey because of the uncertainty in the absolute magnitude of observed Cepheids.

From the evolutionary calculations of 5–$15M_\odot$ it is known that they cross the Cepheid strip at least once in their evoultion up the red giant branch. Although there is not a unique mass–luminosity relation when a given star crosses the strip more than once, usually one crossing is considerably longer than the others so that the majority of observed Cepheids are likely to satisfy some mass–luminosity relation. Hence with each mass we have associated a single luminosity (since the tracks are almost horizontal across the strip) corresponding to the crossing of longest duration and these values are listed in Table I.

TABLE I

Mass–luminosity relation of classical Cepheids from evolutionary calculations

$M/M_\odot$	$L/L_\odot$
5	1000
6	2500
7	5000
9	10 000

The luminosity for $M/M_\odot = 6$ is an interpolation between the $5M_\odot$ and $7M_\odot$ values since no star of this mass was evolved up the red giant branch. The range in luminosity corresponds to a range in M_{bol} of $2^m{\cdot}5$ which covers most of the observed strip. Hofmeister (1967) has shown that these evolutionary tracks depend on the

Downloaded from https://academic.oup.com/mnras/article/144/4/485/2602797 by guest on 21 August 2022

© Royal Astronomical Society • Provided by the NASA Astrophysics Data System

1969MNRAS.144..485S

value of the heavy element content, Z. The lower Z is the lower the luminosity at which a given star crosses the strip and the second and higher crossings may no longer exist. The above mass–luminosity relation corresponds to $Z = 0{\cdot}044$.

In order to determine the effect of helium content on the position of the strip, we have examined the three compositions indicated in Table II, all with heavy element content $Z = 0{\cdot}04$. We have examined for instability models satisfying the mass–luminosity relation of Table I with the three chemical compositions of Table II. Implicit in this is the assumption that the helium content does not affect the mass–luminosity relationship. Our conclusions concerning the effect of helium content on the position of the instability strip could be affected by this assumption.

TABLE II

X	Y
0·81	0·15
0·66	0·30
0·51	0·45

Given the chemical composition and the particular combination of mass and luminosity, a sequence of models of different T_e were run across the strip. As the observed strip appears to be not wider than $\Delta(B-V) = 0^{m}{\cdot}3$ (corresponding roughly to 700°K), the unstable models which were examined over a range of ~ 1000°K should adequately cover the strip. Moreover to examine models at lower effective temperatures is not worthwhile since convection begins to transport a large fraction of the total flux in the atmosphere. The difference in T_e from one model to the next was chosen to be 300°K since this value gave 3 or 4 unstable models for each sequence and also enabled the left hand edge of the strip to be determined fairly accurately.

The static parameters of the models in the survey are listed in Table III. For each model we have given its mass, luminosity, effective temperature, radius and bolometric magnitude. The mass, luminosity and radius of the sun are taken from Allen (1963) and the bolometric magnitude of the sun, $M_{bol} = 4{\cdot}77$, from Stebbins & Kron (1957). The last two columns of the table give the visual magnitude and the colour which are required for any comparison between the observed and theoretical HR diagrams. The visual magnitude and the colour are related to the bolometric magnitude and the effective temperature by the following relations:

$$\log T_e = 3{\cdot}886 - 0{\cdot}175(B-V), \quad 0{\cdot}30 \leqslant (B-V) \leqslant 1{\cdot}15$$

$$M_{bol} - M_v = -0{\cdot}116 + 0{\cdot}583(B-V) - 0{\cdot}704(B-V)^2$$

taken from Kraft (1961). Although the range of application of these relations is $0{\cdot}30 \leqslant (B-V) \leqslant 1{\cdot}15$ we have assumed that they hold over the range

$$0{\cdot}00 \leqslant (B-V) \leqslant 1{\cdot}23.$$

We have also assumed that these relations, which are essentially derived from Oke's (1961a, b) observations of δ Cephei and η Aquilae, apply over the length of the strip investigated (period range 1–30 days). The slope of the $T_e - (B-V)$ relation is well determined but the zero point of the relation is sensitive to the type of model atmosphere fitted to Oke's results, e.g. the T_e for a given $(B-V)$ can be lowered by about 150°K if line effects are included in the model atmosphere calculations. The second equation, over the range of $(B-V)$ we are interested in, gives bolometric

Downloaded from https://academic.oup.com/mnras/article/144/4/485/2602797 by guest on 21 August 2022

© Royal Astronomical Society • Provided by the NASA Astrophysics Data System

1969MNRAS.144..485S

TABLE III

Parameters of static models in the main survey

Star	$M/M_\odot$	$L/L_\odot$	T_e	$R/R_\odot$	M_{bol}	M_V	$B-V$
1a	5	1000	7700	17·93	−2·730	−2·61	0·00
1b	5	1000	7400	19·41	−2·730	−2·67	0·10
1c	5	1000	7100	21·09	−2·730	−2·70	0·20
1d	5	1000	6800	22·99	−2·730	−2·73	0·30
1e	5	1000	6500	25·16	−2·730	−2·72	0·42
1f	5	1000	6200	27·66	−2·730	−2·71	0·54
1g	5	1000	5900	30·54	−2·730	−2·68	0·66
1h	5	1000	5600	33·90	−2·730	−2·62	0·80
2a	6	2500	6800	36·35	−3·725	−3·72	0·30
2b	6	2500	6500	39·78	−3·725	−3·71	0·42
2c	6	2500	6200	43·73	−3·725	−3·70	0·54
2d	6	2500	5900	48·29	−3·725	−3·67	0·66
2e	6	2500	5600	53·60	−3·725	−3·61	0·80
3a	7	5000	6500	56·26	−4·477	−4·47	0·42
3b	7	5000	6200	61·84	−4·477	−4·46	0·54
3c	7	5000	5900	68·29	−4·477	−4·43	0·66
3d	7	5000	5600	75·80	−4·477	−4·37	0·80
3e	7	5000	5300	84·62	−4·477	−4·30	0·93
3f	7	5000	5000	95·08	−4·477	−4·18	1·08
3g	7	5000	4700	107·6	−4·477	−4·04	1·23
4a	9	10 000	5900	96·57	−5·230	−5·18	0·66
4b	9	10 000	5600	107·2	−5·230	−5·12	0·80
4c	9	10 000	5300	119·7	−5·230	−5·05	0·93
4d	9	10 000	5000	134·5	−5·230	−4·93	1·08
4e	9	10 000	4700	152·2	−5·230	−4·79	1·23

corrections varying from $0^m{\cdot}0$ to $-0^m{\cdot}3$ so that even if the bolometric corrections are not accurate they are small enough not to substantially affect the comparison of the HR diagrams.

3. RESULTS OF THE SURVEY

In Table IV we present the full amplitude results of the stars in Table III, examined with the three different chemical compositions of Table II. The mode is 0, 1 or 2 depending on whether the motion was initiated with a fundamental, first or second mode velocity distribution. The stability of a given star will be explained in Section 4. The period (in days) and its standard deviation were calculated from the last three cycles of the motion for, because of the decay of the transients initially generated, the standard deviation is in general smaller than the standard deviation calculated from the whole motion. The period calculated is on average accurate to 3 per cent. The parameters of the next six columns, namely the velocity amplitude, the bolometric magnitude amplitude, the effective temperature amplitude, the total radius variation, the velocity asymmetry and the phase lag were also all calculated by averaging over the last three periods of the motion. The reason for averaging over this number of periods was to minimize the effect of unwanted modes which, in general, were present in the full amplitude motion. The parameter describing the velocity asymmetry is the ratio of the time spent on the descending part of the velocity curve (in the theoretical sense, i.e. relative to the centre of the star) to the time spent on the ascending part. The phase lag is the delay, measured as a fraction of a period, by which the luminosity curve passing through its static value on the ascending branch lags behind the velocity curve passing through zero velocity on its ascending

Downloaded from https://academic.oup.com/mnras/article/144/4/485/2602797 by guest on 21 August 2022

© Royal Astronomical Society • Provided by the NASA Astrophysics Data System

1969MNRAS.144..485S

TABLE IV

Full amplitude results of main survey

Star	Mode	Stable	$P \pm \Delta P$	V_R	ΔM_{bol}	ΔT_e	ΔR	V_{asy}	Lag	Bump
$X = 0{\cdot}81$, $Y = 0{\cdot}15$										
1e	2	+								
1f	2	+								
1e	1	+								
1f	1	−	$1{\cdot}8 \pm 0{\cdot}1$							
1g	1	−	$2{\cdot}3 \pm 0{\cdot}2$							
1h	1	−	$2{\cdot}6 \pm 0{\cdot}1$							
1h	0	+								
3d	1	+								
3e	1	+								
3d	0	+								
3e	0	−	$12{\cdot}6 \pm 0{\cdot}5$	28	$0{\cdot}58$	750	$4{\cdot}310^{11}$	$1{\cdot}88$	$0{\cdot}01$	D
6f	0	−	$15{\cdot}3 \pm 0{\cdot}4$	37	$0{\cdot}65$	800	$6{\cdot}310^{11}$	$2{\cdot}82$	$0{\cdot}02$	D
3g	0	−	$19{\cdot}9 \pm 0{\cdot}1$	77	$1{\cdot}85$	1650	$1{\cdot}68_{10}12$	$1{\cdot}18$	$0{\cdot}15$	A
4b	1	+								
4c	1	+								
4b	0	+								
4c	0	−	$19{\cdot}6 \pm 0{\cdot}3$	23	$0{\cdot}51$	560	$5{\cdot}310^{11}$	$2{\cdot}54$	$-0{\cdot}06$	D
4d	0	−	$24{\cdot}6 \pm 0{\cdot}3$	51	$1{\cdot}15$	1320	$1{\cdot}3310^{12}$	$1{\cdot}10$	$0{\cdot}07$	A
4e	0	−	$30{\cdot}4 \pm 1{\cdot}9$	73	$1{\cdot}80$	1730	$2{\cdot}7210^{12}$	$2{\cdot}24$	$0{\cdot}10$	A
$X = 0{\cdot}66$, $Y = 0{\cdot}30$										
1c	2	+								
1d	2	+								
1e	2	+								
1c	1	*	$1{\cdot}2 \pm 0{\cdot}2$							
1e	1	*	$1{\cdot}6 \pm 0{\cdot}3$							
1f	1	*	$1{\cdot}7 \pm 0{\cdot}1$							
1g	1	−	$2{\cdot}1 \pm 0{\cdot}2$	35	$0{\cdot}38$	470	$9{\cdot}410^{10}$	$1{\cdot}83$	$0{\cdot}05$	X
1h	1	−	$2{\cdot}61 \pm 0{\cdot}06$	42	$0{\cdot}55$	680	$1{\cdot}510^{11}$	$2{\cdot}2$	$0{\cdot}05$	X
1g	0	+								
1h	0	*	$3{\cdot}4 \pm 0{\cdot}2$	28	$0{\cdot}40$	420	$1{\cdot}210^{11}$	$1{\cdot}5$	$0{\cdot}12$	X
2a	1	+								
2b	1	+								
2c	1	−	$3{\cdot}5 \pm 0{\cdot}2$	18	$0{\cdot}32$	470	$8{\cdot}910^{10}$	$1{\cdot}5$	$-0{\cdot}15$	X
2d	1	−	$4{\cdot}0 \pm 0{\cdot}1$	28	$0{\cdot}43$	525	$1{\cdot}3510^{11}$	$2{\cdot}5$	$-0{\cdot}05$	X
2e	1	−	$4{\cdot}7 \pm 0{\cdot}1$	29	$0{\cdot}40$	500	$1{\cdot}5410^{11}$	$2{\cdot}23$	$-0{\cdot}08$	X
2e	0	*	$6{\cdot}4 \pm 0{\cdot}5$	32	$0{\cdot}52$	620	$2{\cdot}6_{10}11$	—	—	X
3a	1	+								
3b	1	+								
3c	1	−	$6{\cdot}40 \pm 0{\cdot}05$	27	$0{\cdot}42$	540	$2{\cdot}1510^{11}$	$1{\cdot}75$	$0{\cdot}00$	X
3d	1	−	$7{\cdot}54 \pm 0{\cdot}01$	40	$0{\cdot}65$	750	$3{\cdot}8610^{11}$	$1{\cdot}7$	$0{\cdot}00$	X
3e	1	−	$9{\cdot}26 \pm 0{\cdot}02$	37	$0{\cdot}57$	550	$4{\cdot}3210^{11}$	$1{\cdot}7$	$0{\cdot}00$	X
3c	0	−	$8{\cdot}76 \pm 0{\cdot}09$	22	$0{\cdot}35$	555	$2{\cdot}3410^{11}$	$1{\cdot}4$	$0{\cdot}03$	X
3d	0	−	$10{\cdot}5 \pm 0{\cdot}2$	31	$0{\cdot}46$	640	$4{\cdot}0810^{11}$	$2{\cdot}1$	$0{\cdot}00$	X
3e	0	−	$12{\cdot}6 \pm 0{\cdot}1$	42	$0{\cdot}75$	—	—	$2{\cdot}7$	$0{\cdot}07$	D
3f	0	−	$15{\cdot}8 \pm 0{\cdot}3$	58	$1{\cdot}17$	1090	$9{\cdot}5010^{11}$	$3{\cdot}5$	$0{\cdot}08$	D
4a	1	+								
4b	1	−	$11{\cdot}4 \pm 0{\cdot}4$	23	$0{\cdot}35$	550	$3{\cdot}5210^{11}$	$1{\cdot}5$	—	X
4c	1	*	$14{\cdot}1 \pm 0{\cdot}8$	25	$0{\cdot}45$	530	$4{\cdot}8_{10}11$	$1{\cdot}5$	—	X
4a	0	+								
4b	0	*	$16{\cdot}0 \pm 0{\cdot}3$	26	$0{\cdot}50$	650	$5{\cdot}1610^{11}$	$1{\cdot}5$	$0{\cdot}00$	X
4c	0	−	$19{\cdot}6 \pm 0{\cdot}3$	42	$0{\cdot}85$	810	$8{\cdot}7010^{11}$	$3{\cdot}5$	$0{\cdot}02$	D
4d	0	−	$24{\cdot}2 \pm 0{\cdot}4$	35	$0{\cdot}71$	720	$8{\cdot}1010^{11}$	—	$0{\cdot}08$	M
4e	0	−	$31{\cdot}1 \pm 3{\cdot}1$	85	$1{\cdot}75$	—	—	—	—	A

Downloaded from https://academic.oup.com/mnras/article/144/4/485/2602797 by guest on 21 August 2022

© Royal Astronomical Society • Provided by the NASA Astrophysics Data System

1969MNRAS.144..485S

TABLE IV—*Continued*

Star	Mode	Stable	$P \pm \Delta P$	V_R	ΔM_{bol}	ΔT_e	ΔR	V_{asy}	Lag	Bump
$X = 0{\cdot}51$, $Y = 0{\cdot}45$										
1a	2	+								
1b	2	*								
1c	2	*	$0{\cdot}85 \pm 0{\cdot}07$	30	0·30	—	—	—	—	X
1d	2	−	$1{\cdot}10 \pm 0{\cdot}06$	45	0·70	—	—	2·6	0·00	X
1e	2	−	$1{\cdot}24 \pm 0{\cdot}04$	54	0·50	680	$8{\cdot}4_{10}10$	2·5	0·06	X
1f	2	−	$1{\cdot}44 \pm 0{\cdot}04$	30	0·33	430	$5{\cdot}6_{10}10$	1·7	0·10	X
3a	2	+								
3b	2	+								
3a	1	*	$4{\cdot}7 \pm 0{\cdot}3$	26	0·40	630	$1{\cdot}5_{10}11$	1·7	—	X
3b	1	−	$5{\cdot}6 \pm 0{\cdot}3$	23	0·33	500	$1{\cdot}6_{10}11$	1·6	0·03	X
3c	1	−	$6{\cdot}4 \pm 0{\cdot}2$	35	0·42	540	$2{\cdot}8_{10}11$	2·7	0·07	D
3d	1	−	$7{\cdot}71 \pm 0{\cdot}06$	38	0·70	710	$3{\cdot}6_{10}11$	—	0·13	M
3d	0	*								
4a	1	+								
4b	1	*	$11{\cdot}5 \pm 0{\cdot}3$	50	0·76	800	$7{\cdot}35_{10}11$	2·3	0·02	X
4c	1	*	$14{\cdot}3 \pm 0{\cdot}2$	52	0·80	880	$9{\cdot}28_{10}11$	2·1	0·05	X
4c	0	−	$19{\cdot}8 \pm 0{\cdot}4$	43	0·88	870	$1{\cdot}04_{10}12$	2·8	0·05	D
4d	0	−	$24{\cdot}0 \pm 0{\cdot}4$	57	1·22	1150	$1{\cdot}38_{10}12$	3·5	0·10	D

branch. Hence the conventional $\pi/2$ phase lag corresponds to a zero phase lag as defined here. The particular choice of the other parameters describing the full amplitude motion is explained in Paper I (Stobie, 1969). In the last column of Table IV, the presence of a prominent bump on the velocity curve is indicated by a *X* if no bump, an *A* if bump on ascending branch (in the theoretical sense), an *M* if bump at maximum and a *D* if bump on descending branch.

The results of Table IV are not complete for two reasons. One is that for some unstable stars, particularly with sequence 1 ($M/M_\odot = 5$, $L/L_\odot = 1000$), it was found to be extremely difficult to initiate the star's pulsation with a satisfactory velocity distribution corresponding to the fundamental or first modes. No matter how we changed the parameters of this distribution the ensuing motion contained such a high content of spurious modes that it was not worthwhile following the motion to full amplitude. Initially, we had only considered instability in the fundamental and first modes for the survey but because of these difficulties we were led to suspect instability in another mode and hence we examined velocity distributions of the second mode type. In the case of three stars with composition $X = 0{\cdot}51$, $Y = 0{\cdot}45$ and parameters

$$M/M_\odot = 5, \quad L/L_\odot = 1000, \quad T_e = 6200, 6500, 6800\,^\circ\mathrm{K}$$

this second mode instability was confirmed, for the ensuing motion showed far less contamination of other modes than velocity distributions of the type corresponding to the fundamental or first modes. However, two other stars on this sequence with $T_e = 7100$, $7400\,^\circ$K failed to give satisfactory second mode distributions and these stars were probably unstable in modes higher than the second. In examining the $5M_\odot$ sequence with compositions $X = 0{\cdot}81$, $Y = 0{\cdot}15$ and $X = 0{\cdot}66$, $Y = 0{\cdot}30$ the second mode was found to be stable so that no satisfactory velocity distributions of any type were found. Part of the difficulty lay in the extremely low growth rates and low full amplitudes of these stars, for the initial velocity amplitude was close to the full amplitude. This might well make it impossible to generate a sufficiently pure mode such that the motion to full amplitude can be followed.

Downloaded from https://academic.oup.com/mnras/article/144/4/485/2602797 by guest on 21 August 2022

© Royal Astronomical Society • Provided by the NASA Astrophysics Data System

1969MNRAS.144..485S

A second reason for the incompleteness of the results is that the majority of the stars were unstable to velocity amplitudes not greater than 40 km s^{-1}. This meant that the light curve of the star at full amplitude was unreliable in that it could not be reproduced by a slightly different mass zoning since only one or two mass zones moved through the hydrogen ionization region per period. As described in Section 6 of Paper I we require 4 to 5 mass zones to move through this region per period at full amplitude in order to obtain a reliable light curve. With the mass zoning chosen this condition was in general satisfied for stars which were unstable to more than 50 km s^{-1}. Hence no details of the shape of such light curves have been reproduced and we have only plotted details of the velocity curves. It is unfortunate that the computations should give the velocity curve more accurately than the light curve for in the observations exactly the opposite occurs.

The results of the survey will be further analysed in the following sections.

4. INTERPRETATION OF THE INSTABILITY

The instability of a star is determined by examining the maximum kinetic energy per cycle over the first six periods of the motion. The reason for examining the maximum kinetic energy per cycle is because this parameter is least sensitive to contamination by unwanted modes and in averaging over two consecutive sets of three periods we can approximately eliminate the effects of the unwanted modes. If the average over the first three periods exceeds the average over the second three periods then the star is considered stable to a total amplitude of 20 km s^{-1} (indicated by a '+'). If, on the other hand, the average of the second three periods exceeds that of the first three periods then the star is considered unstable (indicated by a '−') and its motion is then followed to full amplitude as described in Paper I. The situation is clear cut if the star is stable provided that the motion has been generated by a satisfactory velocity distribution. The situation is also clear cut if the star is unstable to only one of the modes examined and stable to the others. However, in many cases it was observed the star appeared, from the first six periods of the motion, to be unstable in two modes. The situation is then more complicated for two possibilities arise. Either (1) the star really is unstable in both modes or (2) the star is unstable to one mode only although initially it appears unstable to both. Ideally, if case (2) arises then generating the star's motion with the velocity distribution to which it is stable would reveal that the star initially appeared unstable, but on following the motion for a large number of periods this mode would gradually decay into the mode to which the star is unstable. Because of the long *e*-folding times of Cepheids this procedure is not practicable as it would take many periods for the motion to degenerate from one mode to the other. Instead we have attempted to distinguish the two possibilities (1) and (2) by examining the period dispersion and the velocity amplitude dispersion as a function of the number of periods after initiation. Both of these parameters are strongly dependent on contamination by modes other than the one being examined. In Fig. 1 we illustrate this dispersion as a function of period number for two stars both of which initially appeared to be unstable. Fig. 1 (a) is a typical case of a star that is definitely unstable to the mode examined for both the period and velocity amplitude dispersion decrease as the number of periods after initiation increases. Fig. 1 (b) shows just the opposite effect and in this case we conclude that although the star initially appears to be unstable to the mode examined, it is really unstable in some other mode. These cases are

Downloaded from https://academic.oup.com/mnras/article/144/4/485/2602797 by guest on 21 August 2022

© Royal Astronomical Society • Provided by the NASA Astrophysics Data System

1969MNRAS.144..485S

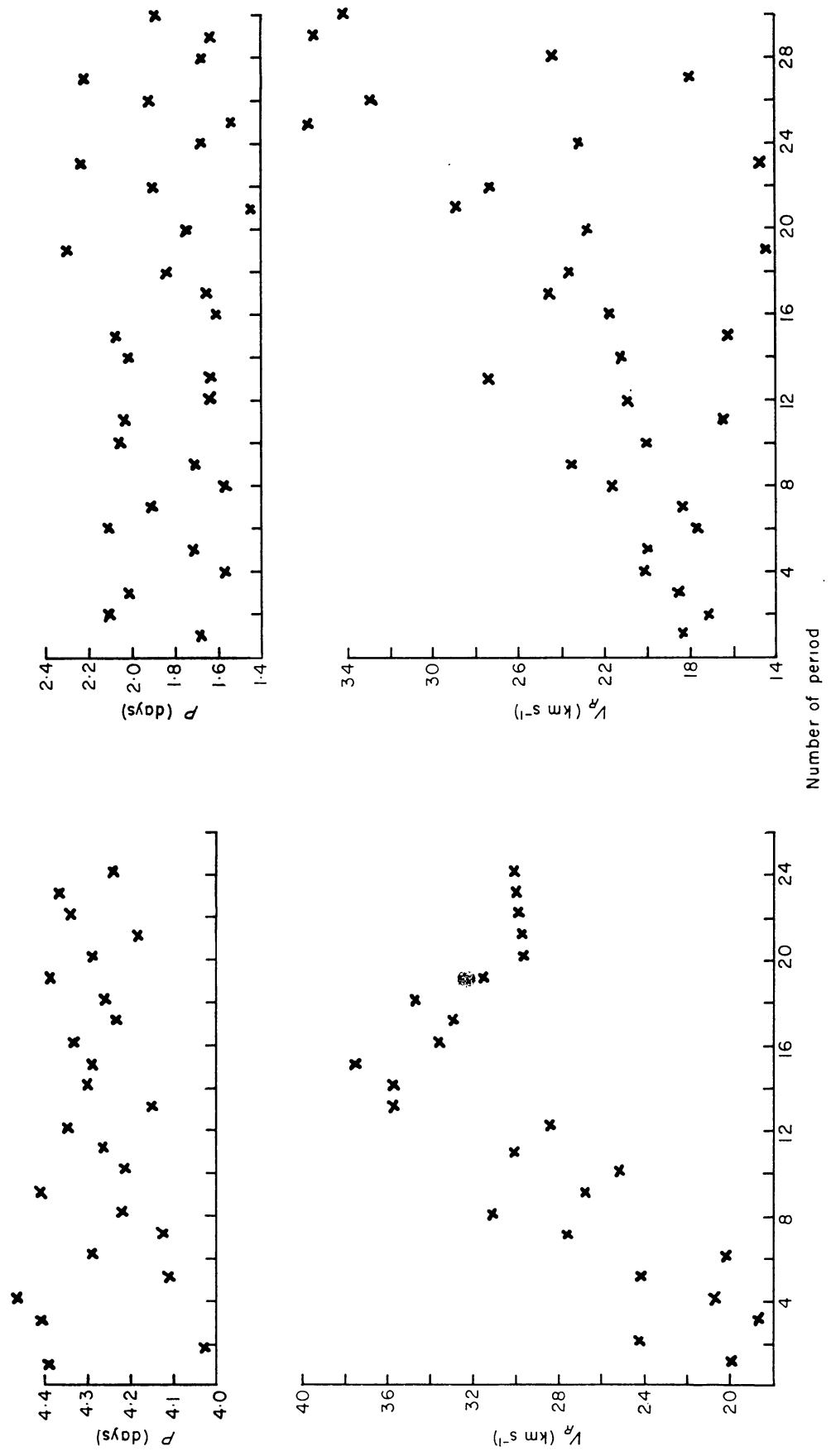

FIG. 1. *Period and velocity amplitude dispersion plots as a function of number of period.*

Downloaded from https://academic.oup.com/mnras/article/144/4/485/2602797 by guest on 21 August 2022

© Royal Astronomical Society • Provided by the NASA Astrophysics Data System

1969MNRAS.144..485S

indicated by * in the stability column of Table IV. Although these stars are almost certainly not unstable to the particular mode examined, the full amplitude results have still been included for completeness. In a few cases, from the dispersion plots it was not obvious whether or not the dispersion decreases and in these situations we have still indicated the instability by a '–'.

5. HERTZSPRUNG–RUSSELL DIAGRAM

From the results of the survey in Table IV we obtain a definite high T_e boundary to the instability but there is no sign of the stars stabilizing at low T_e. Indeed, over the range of effective temperature where unstable models were found, the lower the T_e the greater the maximum amplitude of the model. As this range of T_e is almost twice the width of the observed strip we conclude that stable models at the low T_e boundary of the strip can only be found if the interaction of convection and pulsation is taken into account. The models in the present calculations were purely radiative. This result, that no stabilization was found at low T_e, is in contradiction with that obtained by Cox *et al.* (1966) who found that radiative atmosphere models stabilized on both sides of the strip. We believe this difference arises solely from our inclusion of the destabilizing effects of hydrogen and helium I ionization which contribute proportionately a greater destabilizing influence the lower the effective temperature (corresponding to greater densities in the H and He I ionization zones).

To compare the results with observation, the unstable models have been plotted on an HR diagram in Fig. 2 where the transformations $M_{\rm bol} \rightarrow M_V$ and $T_e \rightarrow (B-V)$ were carried out by means of Kraft's (1961) relations (see Section 2). To avoid confusion in the diagram and also because the observed strip is not wider than $0^{\rm m}\cdot3$ in $(B-V)$ we have only plotted the first two high T_e unstable stars in each sequence. The number above each star in the diagram denotes its period in days. When a star is unstable in both the first and fundamental modes, the pair of numbers indicates the two periods respectively. The effect of the helium content on the strip is striking, for the higher the helium content the further the instability strip shifts to higher T_e, similar to the result Christy (1966a) found in his survey of RR Lyrae variables. The shift for every 15 per cent increase in helium content (by mass) is roughly 600 °K for the $5M_\odot$ and $7M_\odot$ sequences but for the $9M_\odot$ sequence the shift is considerably less.

We have chosen to compare this theoretical HR diagram with the observational HR diagram constructed from the 31 well observed galactic Cepheids of Kraft (1961). This diagram for convenience has been reproduced in Fig. 3. The superscript 'o' in M_V and $(B-V)$ denotes that the observed values have been corrected for reddening and the angle brackets denote that a suitable mean of the values throughout a cycle has been taken. Apart from the five galactic cluster Cepheids there is considerable uncertainty in the absolute magnitude of classical Cepheids. In order to locate these 31 classical Cepheids on an HR diagram Kraft had to assume that the grid of constant period lines on this diagram was the same in both the Galaxy and the SMC. The zero point of this grid for Cepheids in our Galaxy was then fixed by the five galactic cluster Cepheids. In this way, given the period and the unreddened colour of a star, its absolute magnitude can be read off from the HR diagram. If we now compare the HR diagrams in Figs 2 and 3, for the left hand edge of the

Downloaded from https://academic.oup.com/mnras/article/144/4/485/2602797 by guest on 21 August 2022

© Royal Astronomical Society • Provided by the NASA Astrophysics Data System

1969MNRAS.144..485S

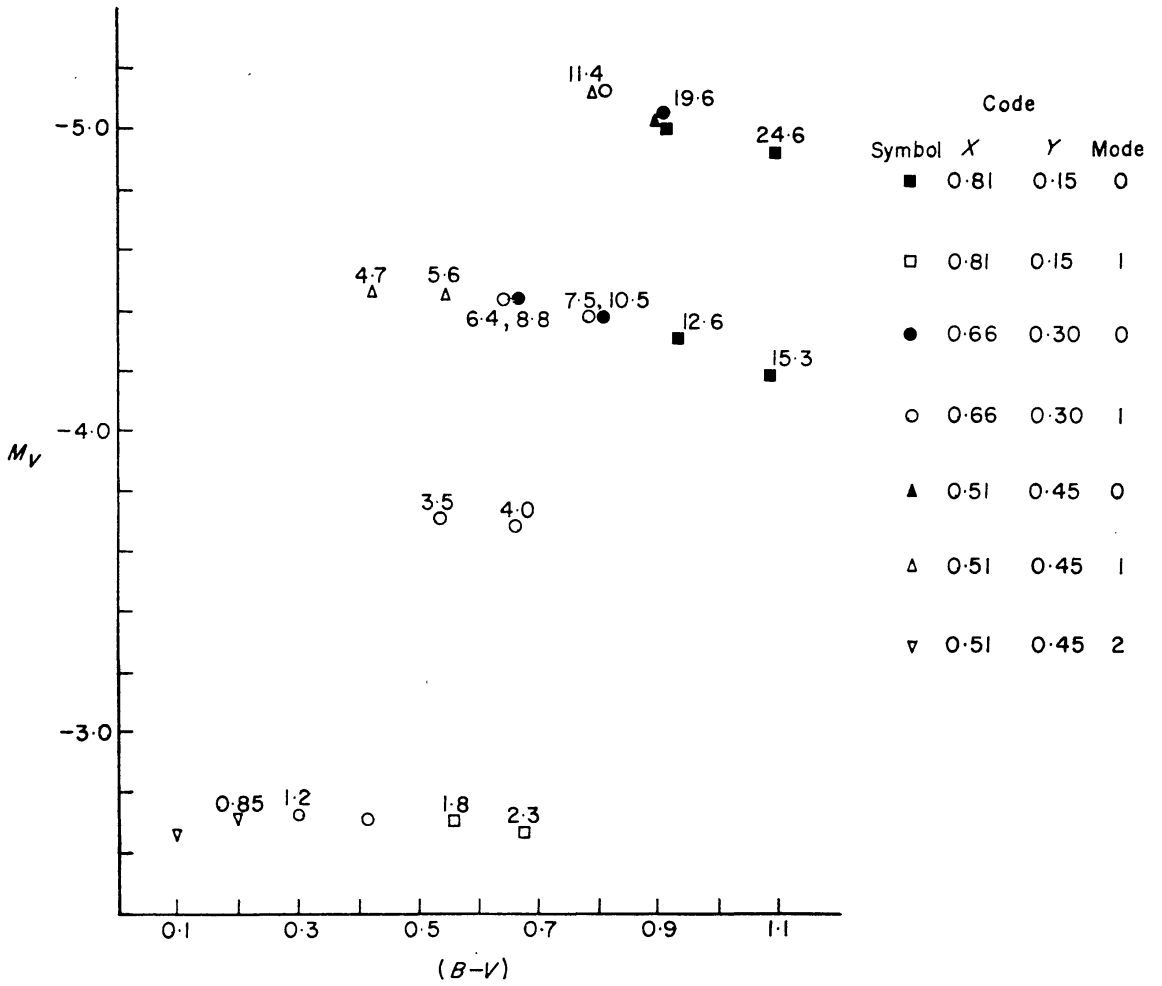

FIG. 2. *The effect of helium content* (Y) *on the HR diagram of classical Cepheids. The models were fitted to the evolutionary tracks of Iben* (1965, 1966*a*, *b*, *c*) *and Hofmeister* (1967). *The transformation of* $M_{bol} \rightarrow M_V$ *and* $T_e \rightarrow (B-V)$ *were carried out by means of Kraft's* (1961) *relations.*

instability strips to agree, the two extreme compositions are ruled out and a composition close to 30 per cent helium would make the best fit. It must be emphasized, however, that there is a large uncertainty associated with this value because of assumptions in the comparison of the HR diagrams. For example, the $T_e-(B-V)$ transformation is derived from Oke's (1961a, b) observations of δ Cephei and η Aquilae. These two stars cover a very small range in period and there is no reason to suppose that this relation will hold for longer or shorter periods.

If we compare the periods at a given M_V and $(B-V)$ in Figs 2 and 3 it is apparent that the periods derived from the models fitted to the evolutionary tracks are consistently too low by a factor of 1·5 compared to the observed periods. To show this more clearly the $M_V - \log P$ plot for the theoretical results has been constructed in Fig. 4 where again we have only included the first two high T_e unstable stars in each sequence. Also plotted are the results of the second survey (Table VI) in order to give a greater density of points. The slope of the relation for the three different compositions is roughly the same and is closer to a value of $-2{\cdot}5$ than $-3{\cdot}0$. This is not considered important for one could obtain different slopes by choosing different

Downloaded from https://academic.oup.com/mnras/article/144/4/485/2602797 by guest on 21 August 2022

© Royal Astronomical Society • Provided by the NASA Astrophysics Data System

1969MNRAS.144..485S

mass distributions along the strip. The significant point is that, with a given mass distribution, the zero point of the relation is quite distinct for the three different compositions and may be approximately represented by the following relations

$$Y = 0{\cdot}15 \quad : \quad M_V = -1{\cdot}9-2{\cdot}5 \log P$$
$$Y = 0{\cdot}30 \quad : \quad M_V = -2{\cdot}4-2{\cdot}5 \log P$$
$$Y = 0{\cdot}45 \quad : \quad M_V = -2{\cdot}9-2{\cdot}5 \log P.$$

To compare with observation we take the relation that Kraft (1961) derived

$$M_V = -1{\cdot}67-2{\cdot}54 \log P,$$

where the slope was obtained from Arp's (1960) observations of SMC Cepheids and the zero point was determined by the five galactic cluster Cepheids. To obtain agreement between the zero points of the theoretical and observational relations we require a considerably lower helium content than that indicated by the position of the instability strip in the HR diagram. Apart from the fact that the assumption of equality in the slope of the relation for the SMC and the Galaxy may not be true,

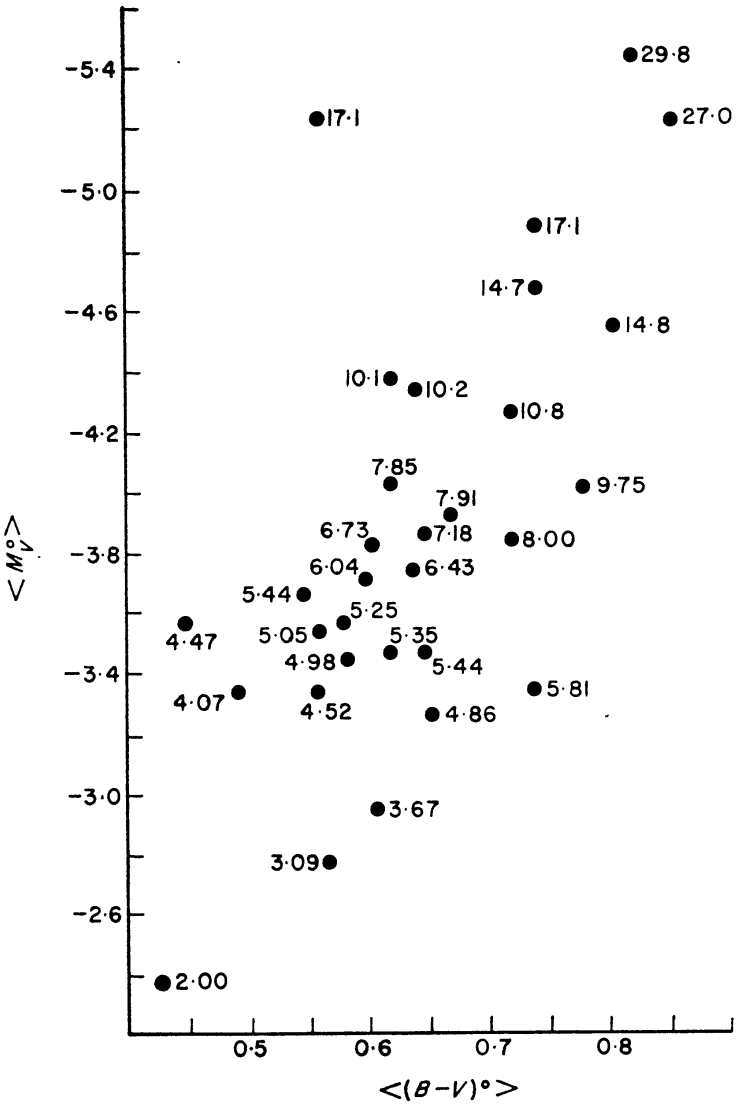

FIG. 3. *HR diagram of the* 31 *field and cluster Cepheids listed by Kraft* (1961).

Downloaded from https://academic.oup.com/mnras/article/144/4/485/2602797 by guest on 21 August 2022

© Royal Astronomical Society • Provided by the NASA Astrophysics Data System

1969MNRAS.144..485S

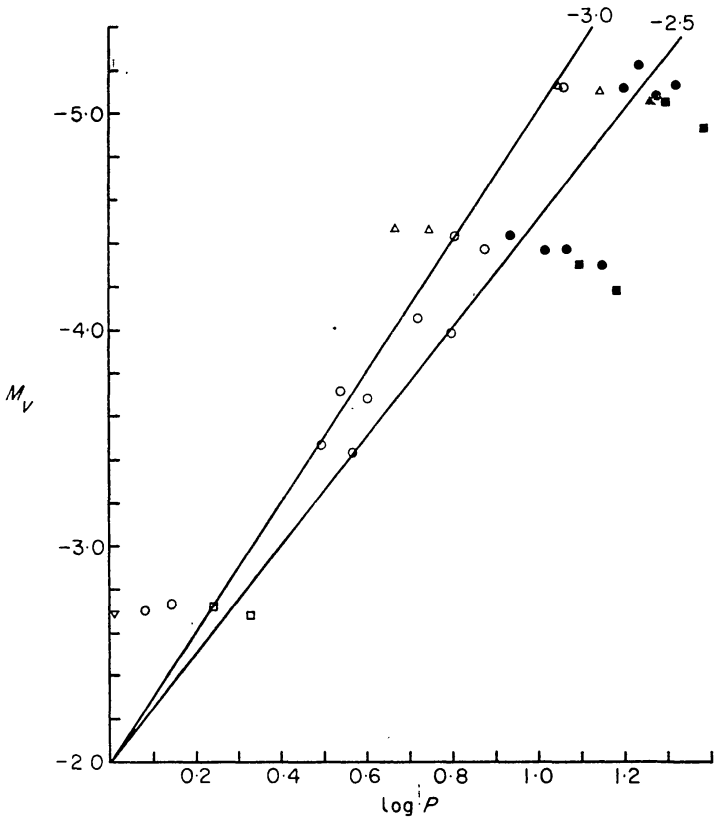

FIG. 4. *This M_V – log P plot is constructed from the first two high T_e unstable stars of each sequence in Tables IV and VI. The two lines drawn represent the slopes −2·5 and −3·0. The code of the diagram is identical to that of Fig. 2.*

there is also some uncertainty as to the value of this slope. Gascoigne & Kron (1965) in their photo-electric observations of SMC Cepheids quote a value of −2·97. This value, however, would make the disagreement even more pronounced since Kraft's relation would then become

$$M_V = -1{\cdot}24-2{\cdot}97 \log P.$$

This discrepancy is not likely to be resolved by uncertainties in the $M_{bol}-M_V$ and the $T_e-(B-V)$ relations for the bolometric correction are small in this region of the HR diagram and the latter relation would have to be out by ~600 °K for the periods at a given M_V to agree. By far the principal uncertainty lies in the absolute magnitude of classical Cepheids which rests solely on the five cluster Cepheids. It is possible that the observed absolute magnitudes could be so far out (~$0^m{\cdot}5$) as to cause this disagreement. The only other way in which this discrepancy can be resolved is to lower the mass for a given luminosity thus increasing the period. It is shown in Section 7 how one can distinguish between these two possibilities in order to resolve the discrepancy.

6. VELOCITY AMPLITUDES

To compare the amplitudes of the models in Table IV with observation, we have chosen to compare the velocity amplitude since in the computations this is more accurately calculated than the light amplitude. The observational results have been taken from the work of Joy (1937) and Stibbs (1955) on the velocity amplitudes of

Downloaded from https://academic.oup.com/mnras/article/144/4/485/2602797 by guest on 21 August 2022

© Royal Astronomical Society • Provided by the NASA Astrophysics Data System

1969MNRAS.144..485S

TABLE V

Parameters of static models in the second survey

Star	$M/M_\odot$	$L/L_\odot$	T_e	$R/R_\odot$	M_{bol}	M_V	$B-V$
5a	5	2000	6200	39·11	−3·483	−3·46	0·54
5b	5	2000	5900	43·19	−3·483	−3·43	0·66
5c	5	2000	5600	47·94	−3·483	−3·37	0·80
5d	5	2000	5300	53·52	−3·483	−3·30	0·93
6a	6	3500	6200	51·74	−4·090	−4·07	0·54
6b	6	3500	5900	57·13	−4·090	−4·04	0·66
6c	6	3500	5600	63·42	−4·090	−3·98	0·80
6d	6	3500	5300	70·80	−4·090	−3·91	0·93
7a	6	5000	5900	68·29	−4·477	−4·43	0·66
7b	6	5000	5600	75·80	−4·477	−4·37	0·80
6c	6	5000	5300	84·62	−4·477	−4·30	0·93
7d	6	5000	5000	95·08	−4·477	−4·18	1·08
8a	8	10 000	5900	95·57	−5·230	−5·18	0·66
8b	8	10 000	5600	107·2	−5·230	−5·12	0·80
8c	8	10 000	5300	119·7	−5·230	−5·05	0·93
8d	8	10 000	5000	134·5	−5·230	−4·93	1·08

TABLE VI

Full amplitude results of second survey

$X = 0{\cdot}66$, $Y = 0{\cdot}30$

Star	Mode	Stable	$P \pm \Delta P$	V_R	ΔM_{bol}	ΔR_e	ΔR	V_{asy}	Lag	Bump
5a	1	−	3·14±0·09	28	0·40	550	1·3 10 11	1·7	0·00	X
5b	1	−	3·71±0·11	34	0·44	570	1·6 10 11	1·8	0·02	X
5c	1	−	4·40±0·06	37	0·50	530	2·0 10 11	1·5	0·08	X
5a	0	+								
5b	0	*	4·5±0·9							
5c	0	−	5·9±0·1	35	0·72	810	2·7 10 11	2·0	0·04	X
5d	0	−	7·3±0·2	49	0·89	810	4·5 10 11	2·8	0·05	X
6a	1	+								
6b	1	−	5·3±0·1	25	0·32	440	1·5 10 11	2·2	−0·08	X
6c	1	−	6·3±0·2	36	0·60	710	2·5 10 11	1·1	−0·09	A
6d	1	*	7·5±0·2							
6a	0	+								
6b	0	+								
6c	0	*	8·5±0·3	37	0·73	820	3·9 10 11	—	—	X
6d	0	−	10·4±0·2	36	0·80	810	4·3 10 11	3·3	0·08	D
7a	1	+								
7b	1	+								
7c	1	+								
7a	0	+								
7b	0	−	11·7±0·4	35	0·60	760	4·8 10 11	2·3	−0·01	D
7c	0	−	14·1±0·2	42	0·77	780	6·6 10 11	3·5	0·05	D
7d	0	−	17·7±0·1	63	1·30	—	—	1·1	0·20	A
8a	0	+								
8b	0	*	17·4±0·4	27	0·50	695	5·6 10 11	2·1	0·00	D
8c	0	−	21·3±0·9	34	0·62	670	8·6 10 11	—	0·05	M
8d	0	−	26·4±1·6	82	1·75	1740	2·4 10 12	2·5	0·02	A

Cepheids in the solar neighbourhood. In Figs 5(a) and (b) we have constructed hodographs of these results to illustrate the velocity amplitude to be expected in a given period range (multiplying the observed amplitudes by a factor 24/17 to convert to radial velocity amplitude). Clearly for periods less than 10 days, by far the

Downloaded from https://academic.oup.com/mnras/article/144/4/485/2602797 by guest on 21 August 2022

© Royal Astronomical Society • Provided by the NASA Astrophysics Data System

1969MNRAS.144..485S

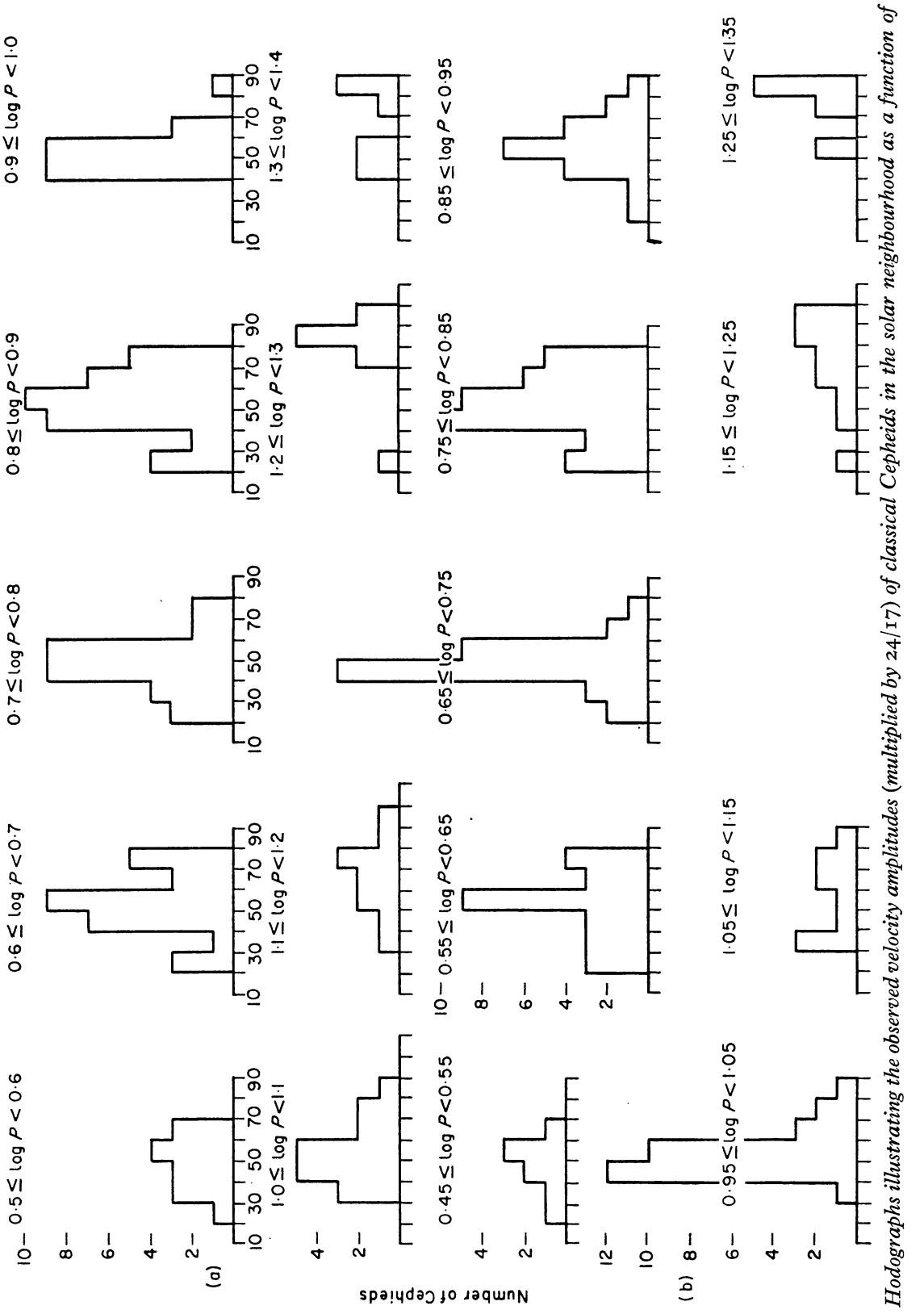

FIG. 5. *Hodographs illustrating the observed velocity amplitudes (multiplied by 24/17) of classical Cepheids in the solar neighbourhood as a function of period.*

Downloaded from https://academic.oup.com/mnras/article/144/4/485/2602797 by guest on 21 August 2022

© Royal Astronomical Society • Provided by the NASA Astrophysics Data System

1969MNRAS.144..485S

majority of observed Cepheids lie in the velocity range 40–60 km s^{-1}. If we examine the theoretical results in Table IV it is apparent that the stars in this period range do not have velocity amplitudes greater than 40 km s^{-1} except for the few stars unstable in the second mode. However, for periods greater than 10 days velocity amplitudes are obtained which compare favourably with the observed values provided low enough effective temperatures are taken. For example, in the sequence 3a–f with composition $X = 0{\cdot}66$, $Y = 0{\cdot}30$ the expected velocity amplitudes are obtained if the strip is at least 1000°K wide. This width is greater than the observed width (~ 700°K) and even if it were possible we should expect a far higher proportion of low amplitude Cepheids than observed among the stars of period greater than 10 days.

To attempt to bring the theoretical velocity amplitudes closer to the observed values, sequences with higher L/M ratios than Table III were run. These sequences are listed in Table V and their full amplitude results all with composition $X = 0{\cdot}66$, $Y = 0{\cdot}30$ in Table VI. With the higher L/M sequences the velocity amplitudes at a given period are in general higher than with the lower L/M sequences. However, for periods less than 10 days only one star has an amplitude greater than 40 km s^{-1}. For periods greater than 10 days the sequences show the characteristic behaviour (also present in Table IV) that the first two high T_e unstable stars are of low amplitude and the third star reaches the high amplitudes expected in this period range. Hence the amplitudes are still in general too low and we should have to increase the luminosity for a given mass still further to obtain velocity amplitudes corresponding to the observed ones.

The position of the high temperature edge of the instability strip is affected by the ratio L/M, for as the luminosity increases for a given mass the strip shifts to lower effective temperatures. Exactly the same effect is observed if one decreases the mass for a given luminosity. This can be seen most readily from the $6M_\odot$ and $7M_\odot$ sequences with composition $X = 0{\cdot}66$, $Y = 0{\cdot}30$ and for convenience we list the relevant results in Table VIII.

TABLE VIII

First high T_e unstable star in the $6M_\odot$ and $7M_\odot$ sequences of Tables IV and VI with composition $X=0{\cdot}66$, $Y=0{\cdot}30$

$M/M_\odot$	$L/L_\odot$	T_e	V_R
6	2500	6200	18
6	3500	5900	25
6	5000	5600	35
7	5000	5900	27

The last column in Table VII shows clearly how rapidly the velocity amplitude increases as the ratio L/M increases. This effect could well explain why observed Cepheids in general have greater amplitudes the greater the period since the ratio L/M increases along the strip.

7. SECONDARY BUMP

The presence of a secondary bump on the velocity curves was a prominent feature of many of the models, principally in the fundamental mode. To illustrate the nature of the bump for various models we have plotted graphs of the velocity curves. A corresponding bump at the same phase occurred on the luminosity curve but for reasons already stated (Section 3) this curve has not been plotted.

Downloaded from https://academic.oup.com/mnras/article/144/4/485/2602797 by guest on 21 August 2022

© Royal Astronomical Society • Provided by the NASA Astrophysics Data System

1969MNRAS.144..485S

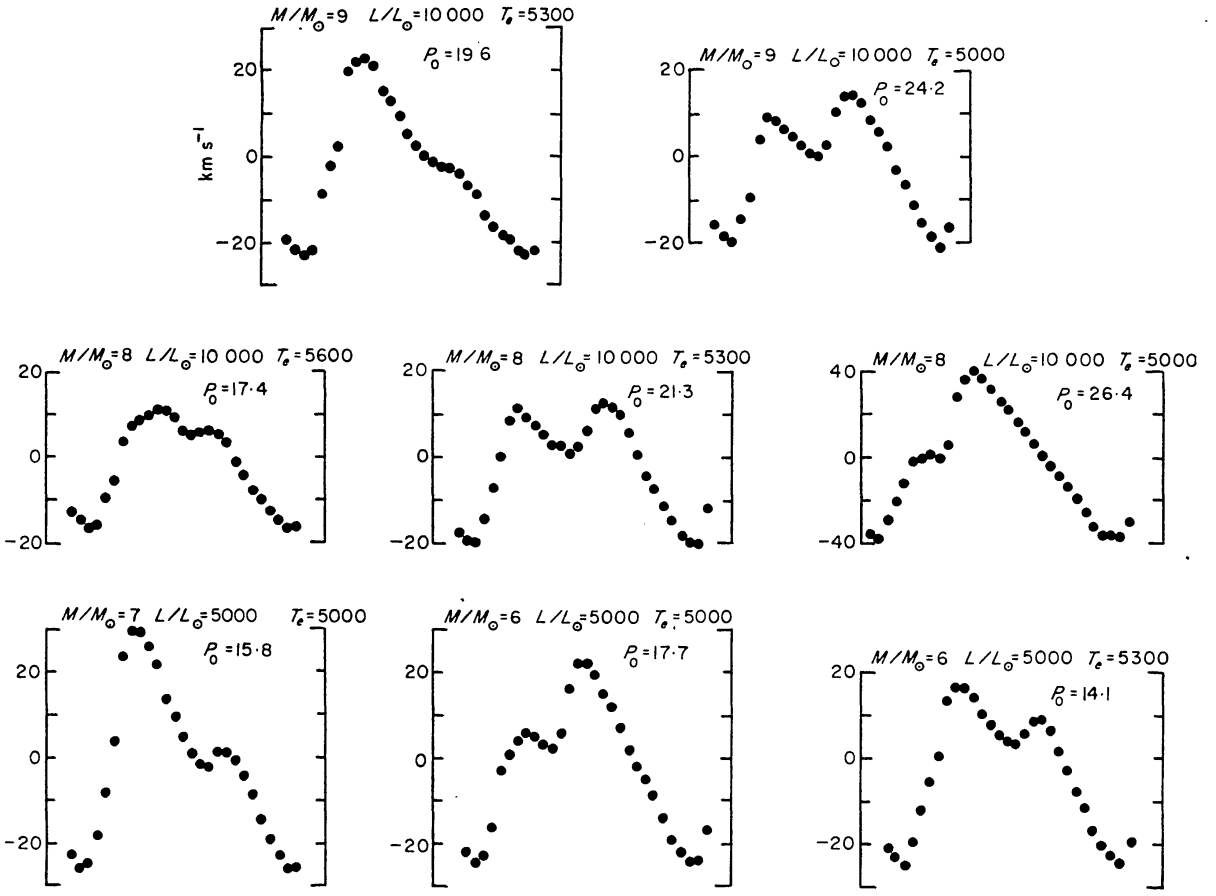

FIG. 6. *Velocity curves illustrating prominent secondary bumps in the fundamental mode. All models have composition* $X = 0{\cdot}66$, $Y = 0{\cdot}30$.

The velocity curves in Fig. 6 exhibit the dependence of the bump on mass, luminosity and effective temperature. The dependence in every case is the same, that is if the parameter we change increases the period then the phase of the bump decreases and vice versa. This is precisely the dependence that is observed in Cepheids. They have a well defined sequence of bumps which may be described as follows. For periods less than six days the curve is smooth. At a period of ~ 7 days a bump appears on the descending branch of the light curve and then decreases in phase as the period increases until the bump coincides with maximum light at a period of ~ 10 days. As the period increases still further the bump continues to decrease in phase moving down the ascending branch until it disappears for periods greater than ~ 17 days. Although there is a dispersion in the phase of the bump at a given period among observed Cepheids, this dispersion is sufficiently small that one can predict quite accurately at what phase a bump will appear given the period. From the curves in Fig. 6 it is apparent that in no case does the bump occur at the phase expected from the observations. In every case the phase of the bump in the models is later than it should be for the given period.

To examine how the phase of the bump can be brought into agreement with observation we have investigated the effect of the chemical composition on the phase. The results are shown in Fig. 7. The top three curves indicate how the helium abundance affects the star $M/M_\odot = 9$, $L/L_\odot = 10\,000$, $T_e = 5000$°K and the bottom three curves indicate the effect of heavy element abundance on the star

© Royal Astronomical Society • Provided by the NASA Astrophysics Data System

Downloaded from https://academic.oup.com/mnras/article/144/4/485/2602797 by guest on 21 August 2022

1969MNRAS.144..485S

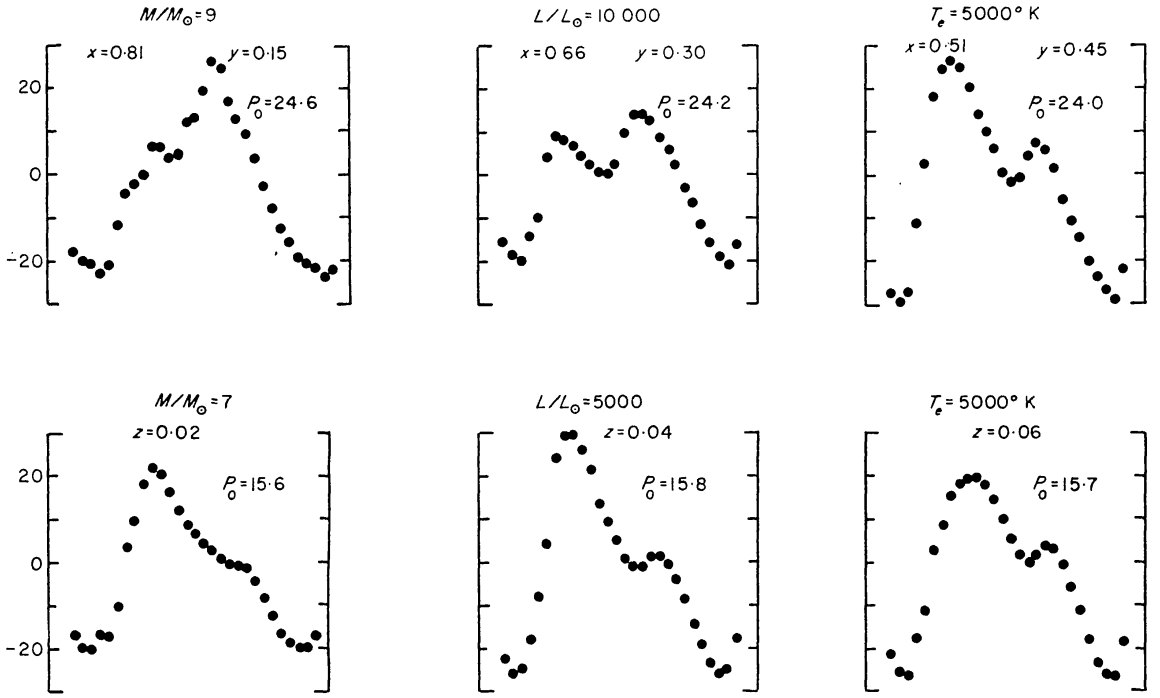

FIG. 7. *Effect of chemical composition on the phase of the bump.*

$M/M_\odot = 7$, $L/L_\odot = 5000$, $T_e = 5000$°K. Although the character of the bump changes slightly with heavy element content, the phase of the bump is quite insensitive to this parameter. However, the helium content does affect the position of the bump in that the lower the helium content the earlier in phase the bump appears. This effect is not nearly great enough to move the position of the bump to the correct phase without having to invoke a negative helium content. Hence to shift the phase of the bump we must examine the results for a differential effect in changing the mass, luminosity and effective temperature. Only a differential effect between two of the above parameters will affect the phase of the bump since each parameter on its own affects the phase in the same way (i.e. depending on whether the period increases or decreases). Such a differential effect can be seen from the three stars listed in Table VIII, the first two of which have a bump coinciding with maximum velocity of expansion and the third which has a bump on the descending branch but occurring extremely close to the maximum. All the stars have the same chemical composition.

TABLE VIII

Models of composition $X = 0{\cdot}66$, $Y = 0{\cdot}30$ *with bump close to maximum velocity of expansion*

$M/M_\odot$	$L/L_\odot$	T_e	P
9	10 000	5000	24·3
8	10 000	5300	21·3
6	5000	5300	14·1

The trend of the results shows that we must consider sequences with considerably higher L/M ratios than indicated by the evolutionary tracks. It is important to realize that this is the only way in which the theoretical results can be brought into agreement with the observations.

Downloaded from https://academic.oup.com/mnras/article/144/4/485/2602797 by guest on 21 August 2022

© Royal Astronomical Society • Provided by the NASA Astrophysics Data System

1969MNRAS.144..485S

As the critical period, where the bump is observed to coincide with maximum light is about 10 days we have examined two sequences which give unstable stars with periods near this critical value. These sequences are $M/M_\odot = 3$, $L/L_\odot = 2500$ and $M/M_\odot = 4$, $L/L_\odot = 2500$ and in Fig. 8 the full amplitude velocity curves have been plotted. For the $4M_\odot$ sequence the critical period is very close to 10 days and for the $3M_\odot$ sequence it is 8·6 days. Because of the dispersion inherent in the observed period-phase of bump relation, it is difficult to distinguish between these two values but it is clear that for the given luminosity the mass cannot lie outside the range 3–$4M_\odot$.

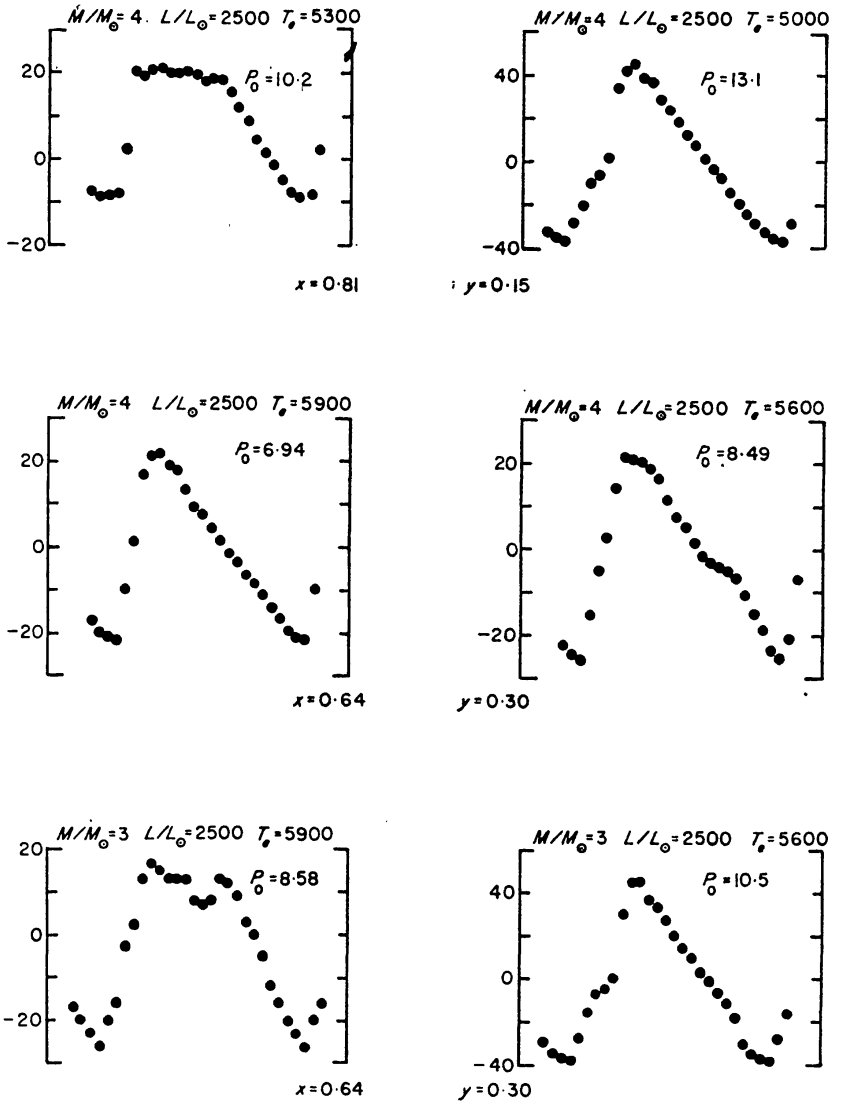

FIG. 8. *Velocity curves illustrating phase of bump for sequences* $M/M_\odot = 3$, $L/L_\odot = 2500$ *and* $M/M_\odot = 4$, $L/L_\odot = 2500$.

It is interesting to compare the above masses with those obtained by Christy (1966c) in constructing models of δ Cephei and η Aquilae. Taking Oke's (1961a, b) observational parameters for these stars, Christy concluded that their masses were

	$M/M_\odot$	$L/L_\odot$
δ Cephei	3·3	1740
η Aquilae	4·2	3590

© Royal Astronomical Society • Provided by the NASA Astrophysics Data System

Downloaded from https://academic.oup.com/mnras/article/144/4/485/2602797 by guest on 21 August 2022

1969MNRAS.144..485S

in order to give agreement with the observed periods. These masses and luminosities agree extremely well with those obtained from fitting the models to the period-phase of bump relation. Christy (1968) examining β Doradus found that, in order to fit the period and the phase of the bump, the required mass was $3{\cdot}4M_{\odot}$ and with the effective temperature derived from observations the luminosity was $3700L_{\odot}$. These results all support the main conclusion of this paper, namely that the masses of classical Cepheids appear to be almost a factor 2 smaller at a given luminosity than the theoretical evolutionary tracks indicate. The only way we know of at present which can reconcile the results of the evolutionary and the pulsation calculations is to assume that Cepheids have suffered mass loss in their evolution from the main sequence to the Cepheid strip (this suggestion was put forward by Christy 1968).

For a given luminosity, reducing the mass affects the position of the instability strip in that the lower the mass the lower the high T_e boundary (see Table VII). Hence it is clear that a third survey with the lower masses is necessary in order to obtain the edge of the instability strip for a given chemical composition. This survey will not be so detailed as the main survey for its purpose is to attempt to narrow down the possible range of helium content and to determine whether the amplitudes of the variables lie in the expected range. The results of this survey will be presented in Paper III of this series.

8. CEPHEID WITH RV TAURI CHARACTERISTICS

In the two surveys carried out only one star was discovered whose full amplitude motion exhibited typical RV Tauri characteristics, i.e. successively shallow and deep minima in the light curve. This dual behaviour was not a result of a quirk of the artificial amplification for, on initiating the motion with a reasonable velocity distribution and no artificial amplification, this motion still developed and persisted. The model which exhibited this behaviour was model 4e in the fundamental mode with composition $X = 0{\cdot}81$, $Y = 0{\cdot}15$. The approach to full amplitude is illustrated in Fig. 9. The maximum kinetic energy cycle shows that the star has been artificially amplified twice and has almost reached full amplitude by period 13. After period 13 the maximum kinetic energy per cycle increases very slowly and for the last 12 periods reveals a separation into two distinct energies. This separation is more pronounced in the velocity amplitude which fluctuates between 65 km s^{-1} and 82 km s^{-1}. The phenomenon is also very pronounced in the period of the motion which alternates between 28·7 and 33·1 days. The period of this star lies in the observed period range covered by RV Tauri variables. It is interesting in this respect to note that the period which satisfies the period–radius–mass relation (this will be derived in Paper III since it includes the results of all three surveys) is the mean of the two periods. Hence the relevant period for pulsation theory in RV Tauri variables is one half of the double cycle. Christy (1966b) found a similar result for his model of W Virginis with RV Tauri characteristics. In Fig. 10 we have plotted the full amplitude light and velocity curves for the double period. These repeat amost identically from one double period to the next. The light maximum varies by $0^{m}{\cdot}25$ from one cycle to the next whereas the light minimum varies by $0^{m}{\cdot}75$.

Christy's RV Tauri variable had a mass of $0{\cdot}88M_{\odot}$, a factor 10 smaller than the mass of the RV Tauri variable considered here. As the observed RV Tauri variables appear to contain certainly Population II and possibly Population I type kinematics one cannot distinguish in this way between the high and low mass or whether indeed

© Royal Astronomical Society • Provided by the NASA Astrophysics Data System

Downloaded from https://academic.oup.com/mnras/article/144/4/485/2602797 by guest on 21 August 2022

1969MNRAS.144..485S

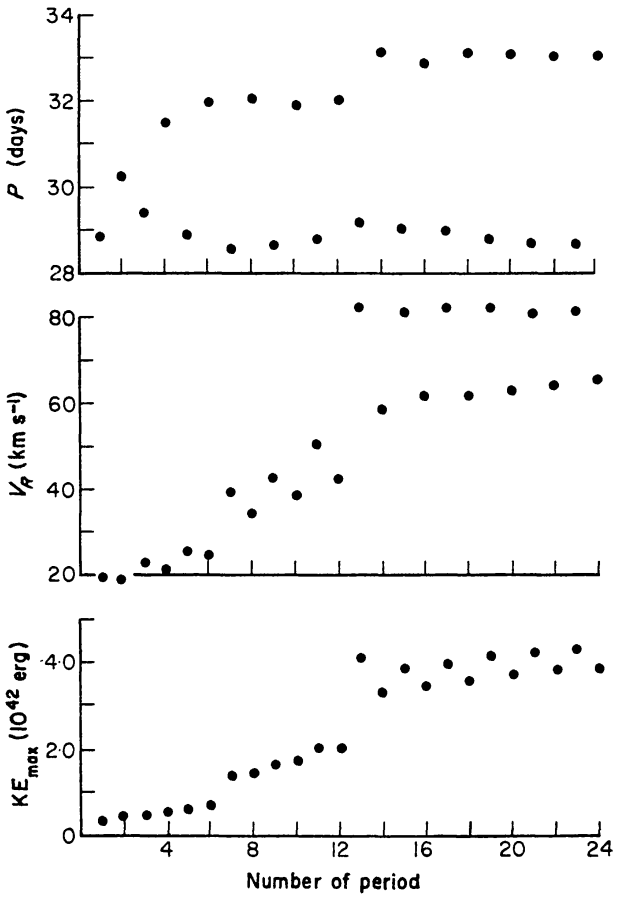

FIG. 9. *RV Tauri variable showing approach to maximum amplitude.*

both give rise to observed RV Tauri variables. However, high dispersion spectrograms have revealed some of the variables to have broken velocity curves which is typical of Population II variables and so would tend to favour the lower mass. Nevertheless, it appears that for a star to exhibit RV Tauri characteristics, it is not necessary for its mass and luminosity to lie in a restricted range. Christy (1968) proposes that RV Tauri behaviour corresponds to low values of the parameter $V_{0.83}$, which is the ratio of the gravitational to thermal energy at relative radius 0·83. As this parameter is roughly proportional to $\sqrt{(M/R)}$, our result is consistent with Christy's suggestion since the value of M/R for the RV Tauri variable discovered here is the lowest of all the models studied in the two surveys.

9. OPACITY

The opacity used in the surveys of classical Cepheids was taken from unpublished tables of Cox & Stewart (1965b). As we wish to vary the chemical composition, four tables were fed in giving a range in composition of $0{\cdot}2 < X < 0{\cdot}8$ and

$$0{\cdot}004 \leqslant Z \leqslant 0{\cdot}06.$$

These four tables are listed in the appendix. To calculate the opacity table for a given composition, log κ was linearly interpolated in X and log Z as suggested by Cox & Stewart (1965a).

Downloaded from https://academic.oup.com/mnras/article/144/4/485/2602797 by guest on 21 August 2022

© Royal Astronomical Society • Provided by the NASA Astrophysics Data System

1969MNRAS.144..485S

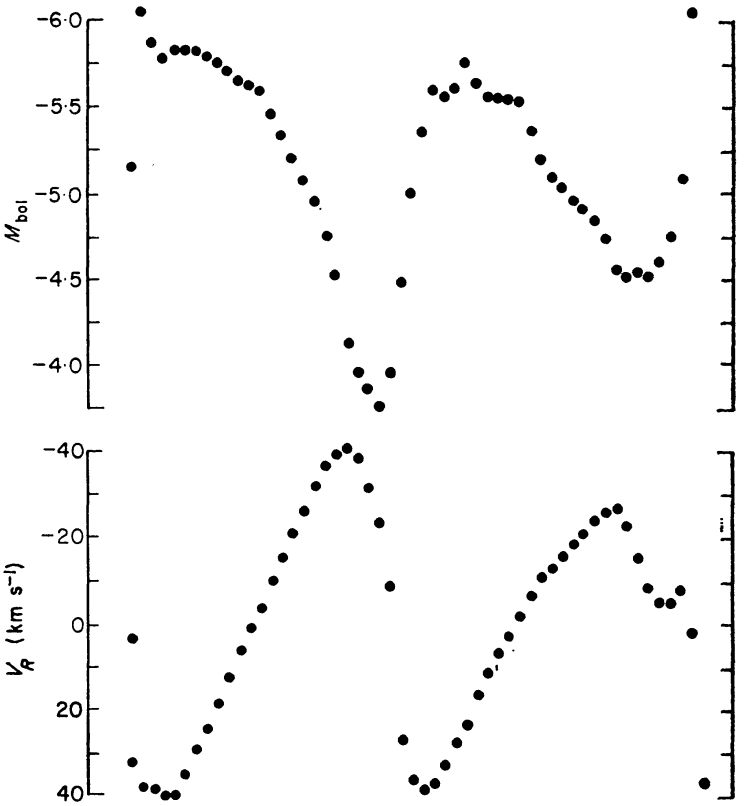

FIG. 10. *Bolometric magnitude and velocity curves of the RV Tauri variable at maximum amplitude.*

ACKNOWLEDGMENTS

I would like to thank Professor R. F. Christy for many valuable discussions. Part of this work was carried out during the tenure of a Science Research Council Studentship.

Institute of Theoretical Astronomy, Madingley Road, Cambridge.

REFERENCES

Allen, C. W., 1963. *Astrophysical Quantities*, 2nd edn, Athlone Press, London.
Arp, H. C., 1960. *Astr. J.*, **65**, 404.
Christy, R. F., 1966a. *Astrophys. J.*, **144**, 108.
Christy, R. F., 1966b. *Astrophys. J.*, **145**, 337.
Christy, R. F., 1966c. *Astrophys. J.*, **145**, 340.
Christy, R. F., 1968. *Q. Jl. R. astr. Soc.*, **9**, 13.
Cox, A. N. & Stewart, J. N., 1965a. *Astrophys. J. Suppl. Ser.*, **94**, 22.
Cox, A. N. & Stewart, J. N., 1965b. Unpublished.
Cox, J. P., Cox, A. N., Olsen, K. H., King, D. S. & Eilers, D. D., 1966. *Astrophys. J.*, **144**, 1038.
Gascoigne, S. C. B. & Kron, G. E., 1965. *Mon. Not. R. astr. Soc.*, **130**, 333.
Hofmeister, E., 1967. *Z. Astrophys.*, **65**, 194.
Iben, I., 1965. *Astrophys. J.*, **142**, 1447.
Iben, I., 1966a. *Astrophys. J.*, **143**, 483.
Iben, I., 1966b. *Astrophys. J.*, **143**, 505.
Iben, I., 1966c. *Astrophys. J.*, **143**, 516.
Joy, A. H., 1937. *Astrophys. J.*, **86**, 363.

Downloaded from https://academic.oup.com/mnras/article/144/4/485/2602797 by guest on 21 August 2022

© Royal Astronomical Society • Provided by the NASA Astrophysics Data System

1969MNRAS.144..485S

Kraft, R. P., 1961. *Astrophys. J.*, **134,** 616.
Oke, J. B., 1961a. *Astrophys. J.*, **133,** 90.
Oke, J. B., 1961b. *Astrophys. J.*, **134,** 214.
Stebbins, J. & Kron, G. E., 1957. *Astrophys. J.*, **126,** 266.
Stibbs, D. W. N., 1955. *Mon. Not. R. astr. Soc.*, **115,** 365.
Stobie, R. S., 1968. *Mon. Not. R. astr. Soc.*, **144,** 461.

APPENDIX

The four opacity tables listed below are unpublished results of Cox & Stewart (1965b) These opacities include the effects of lines and electron conduction and are tabulated as a function of temperature and specific volume. The unit of the opacity is $cm^2\,g^{-1}$.

Downloaded from https://academic.oup.com/mnras/article/144/4/485/2602797 by guest on 21 August 2022

© Royal Astronomical Society • Provided by the NASA Astrophysics Data System

1969MNRAS.144..485S

APPENDIX I

$X = 0{\cdot}800$, $Y = 0{\cdot}196$, $Z = 0{\cdot}004$

V(cm^3 gm^{-1})

T(°K)	1·00+12	1·00+11	1·00+10	1·00+09	1·00+08	1·00+07	1·00+06	1·00+05	1·00+04	1·00+03	1·00+02	1·00+01	1·00+00	1·00−01
1·00+06	—	—	—	—	—	—	3·61−01	3·81−01	4·65−01	1·19+00	6·90+00	2·87+01	8·15+01	2·23+02
5·00+05	—	—	—	—	—	3·62−01	3·83−01	5·25−01	1·68+00	1·13+01	4·48+01	1·25+02	5·57+02	2·00+02
2·00+05	—	—	—	—	3·74−01	4·93−01	1·40+00	1·07+01	1·02+02	5·31+02	1·72+03	2·20+03	—	—
1·00+05	—	—	—	—	6·05−01	2·08+00	1·74+01	2·16+02	2·53+03	1·55+04	2·53+04	9·37+03	—	—
7·00+04	—	—	—	4·61−01	1·04+00	7·01+00	8·18+01	9·63+02	8·19+03	3·64+04	3·56+04	—	—	—
5·00+04	—	—	—	7·28−01	3·46+00	3·46+01	3·50+02	3·64+03	2·81+04	1·15+05	5·80+04	—	—	—
3·00+04	—	—	5·67−01	1·30+00	8·07+00	8·99+01	1·12+03	1·17+04	7·47+04	1·13+05	—	—	—	—
2·00+04	—	—	6·72−01	2·68+00	2·47+01	2·74+02	2·57+03	1·23+04	2·92+04	3·87+04	8·63+03	—	—	—
1·50+04	—	—	1·21+00	7·65+00	7·74+01	6·11+02	2·11+03	4·25+03	7·78+03	1·57+04	2·72+04	—	—	—
1·20+04	—	—	2·59+00	2·18+01	1·24+02	3·27+02	5·89+02	1·04+03	2·11+03	4·91+03	—	—	—	—
1·00+04	—	—	4·67+00	1·91+01	4·04+01	6·81+01	1·23+02	2·49+02	5·96+02	1·45+03	—	—	—	—
9·00+03	—	1·09+00	3·50+00	7·34+00	1·23+01	2·19+01	4·39+01	1·05+02	2·77+02	—	—	—	—	—
8·00+03	—	7·47−01	1·07+00	1·60+00	2·78+00	5·67+00	1·40+01	3·66+01	1·05+02	—	—	—	—	—
7·00+03	—	1·70−01	1·58−01	2·46−01	5·25−01	1·31+00	3·58+00	1·06+01	3·04+01	—	—	—	—	—
6·00+03	3·61−02	1·68−02	1·11−02	2·34−02	6·79−02	2·15−01	6·91−01	2·24+00	—	—	—	—	—	—
5·00+03	2·42−03	1·18−03	1·26−03	2·80−03	8·11−03	2·76−02	1·13−01	4·21−01	—	—	—	—	—	—
4·00+03	9·13−05	5·73−05	6·86−05	2·33−04	1·33−03	6·25−03	2·30−02	6·44−02	—	—	—	—	—	—
3·00+03	1·39−05	1·54−05	2·11−05	3·85−05	1·17−04	4·64−04	1·61−03	4·81−03	—	—	—	—	—	—
2·50+03	9·13−06	9·79−06	1·26−05	1·84−05	3·21−05	7·34−05	1·68−04	3·71−04	—	—	—	—	—	—
1·50+03	7·36−07	6·08−07	6·90−07	9·12−07	1·27−06	1·79−06	2·54−06	3·55−06	—	—	—	—	—	—

Downloaded from https://academic.oup.com/mnras/article/144/4/485/2602797 by guest on 21 August 2022

© Royal Astronomical Society • Provided by the NASA Astrophysics Data System

1969MNRAS.144..485S

APPENDIX II

$X = 0{\cdot}200$, $Y = 0{\cdot}796$, $Z = 0{\cdot}004$

V(cm^3 gm^{-1})

T(°K)	1·00+12	1·00+11	1·00+10	1·00+09	1·00+08	1·00+07	1·00+06	1·00+05	1·00+04	1·00+03	1·00+02	1·00+01	1·00+00	1·00−01
1·00+06	—	—	—	—	—	—	2·42−01	2·57−01	3·36−01	9·45−01	6·21+00	2·78+01	6·84+01	2·60+02
5·00+05	—	—	—	—	—	2·44−01	2·67−01	4·28−01	1·66+00	1·22+01	5·69+01	1·79+02	4·43+01	—
2·00+05	—	—	—	—	2·63−01	4·25−01	1·66+00	1·52+01	1·44+02	1·01+03	4·31+03	4·23+03	—	—
1·00+05	—	—	—	—	4·18−01	1·26+00	1·13+01	1·52+02	1·93+03	2·03+04	5·02+04	1·55+04	—	—
7·00+04	—	—	—	3·01−01	6·44−01	4·18+00	4·85+01	6·19+02	5·14+03	3·34+04	7·50+04	1·43+04	—	—
5·00+04	—	—	—	4·61−01	2·16+00	2·03+01	1·44+02	1·08+03	9·98+03	7·25+04	8·93+04	—	—	—
3·00+04	—	—	2·67−01	4·59−01	2·19+00	2·20+01	2·36+02	2·15+03	1·27+04	4·78+04	1·59+04	—	—	—
2·00+04	—	—	2·62−01	8·52−01	6·05+00	4·38+01	2·63+02	1·61+03	5·43+03	1·19+04	1·14+04	—	—	—
1·50+04	—	—	3·82−01	1·20+00	6·32+00	5·39+01	3·11+02	8·06+02	1·56+03	3·12+03	7·08+03	—	—	—
1·20+04	—	—	2·68−01	1·60+00	1·26+01	5·23+01	1·14+02	2·06+02	4·05+02	8·95+02	—	—	—	—
1·00+04	—	—	4·22−01	2·32+00	6·98+00	1·35+01	2·28+01	4·67+01	1·02+02	2·62+02	—	—	—	—
9·00+03	—	1·48−01	4·49−01	1·27+00	2·31+00	4·10+00	7·84+00	1·71+01	4·52+01	—	—	—	—	—
8·00+03	—	1·42−01	2·21−01	3·24−01	5·13−01	9·40−01	2·27+00	5·79+00	1·66+01	—	—	—	—	—
7·00+03	—	5·24−02	3·91−02	4·61−02	8·37−02	2·03−01	5·38−01	1·55+00	4·88+00	—	—	—	—	—
6·00+03	1·56−02	6·26−03	3·68−03	3·66−03	9·49−03	2·98−03	9·95−02	3·57−01	—	—	—	—	—	—
5·00+03	1·11−03	4·44−04	2·86−04	4·55−04	1·26−03	4·75−03	2·44−02	1·15−01	—	—	—	—	—	—
4·00+03	3·94−05	2·25−05	2·25−05	6·64−05	3·70−04	1·75−03	7·08−03	2·57−02	—	—	—	—	—	—
3·00+03	7·85−06	7·78−06	9·72−06	1·60−05	4·29−05	1·93−04	8·33−04	2·77−03	—	—	—	—	—	—
2·50+03	5·37−06	5·38−06	6·50−06	9·82−06	1·81−05	4·36−05	1·96−04	2·39−04	—	—	—	—	—	—
1·50+03	6·67−07	5·29−07	5·74−07	7·42−07	1·01−06	1·38−06	1·90−06	2·54−06	—	—	—	—	—	—

Downloaded from https://academic.oup.com/mnras/article/144/4/485/2602797 by guest on 21 August 2022

© Royal Astronomical Society • Provided by the NASA Astrophysics Data System

1969MNRAS.144..485S

Appendix III

$X = 0{\cdot}70$, $Y = 0{\cdot}24$, $Z = 0{\cdot}06$

$V(\mathrm{cm^3\ g^{-1}})$

$T(^\circ\mathrm{K})$	$1{\cdot}00+12$	$1{\cdot}00+11$	$1{\cdot}00+10$	$1{\cdot}00+09$	$1{\cdot}00+08$	$1{\cdot}00+07$	$1{\cdot}00+06$	$1{\cdot}00+05$	$1{\cdot}00+04$	$1{\cdot}00+03$	$1{\cdot}00+02$	$1{\cdot}00+01$	$1{\cdot}00+00$	$1{\cdot}00-01$
$1{\cdot}00+06$	—	—	—	—	—	—	$3{\cdot}50-01$	$3{\cdot}97-01$	$7{\cdot}68-01$	$4{\cdot}45+00$	$4{\cdot}06+01$	$2{\cdot}01+02$	$3{\cdot}10+02$	$3{\cdot}19+02$
$5{\cdot}00+05$	—	—	—	—	—	$3{\cdot}48-01$	$4{\cdot}09-01$	$8{\cdot}65-01$	$5{\cdot}86+00$	$6{\cdot}42+01$	$3{\cdot}11+02$	$4{\cdot}95+02$	$8{\cdot}17+02$	$2{\cdot}69+02$
$2{\cdot}00+05$	—	—	—	—	$3{\cdot}72-01$	$5{\cdot}61-01$	$2{\cdot}21+00$	$2{\cdot}32+01$	$3{\cdot}31+02$	$2{\cdot}23+03$	$4{\cdot}14+03$	$2{\cdot}77+03$	—	—
$1{\cdot}00+05$	—	—	—	—	$6{\cdot}18-01$	$2{\cdot}52+00$	$2{\cdot}20+01$	$3{\cdot}36+02$	$3{\cdot}88+03$	$2{\cdot}18+04$	$3{\cdot}19+04$	$1{\cdot}01+04$	—	—
$7{\cdot}00+04$	—	—	—	$4{\cdot}49-01$	$1{\cdot}13+00$	$8{\cdot}69+00$	$1{\cdot}04+02$	$1{\cdot}27+03$	$1{\cdot}19+04$	$5{\cdot}01+04$	$5{\cdot}06+04$	—	—	—
$5{\cdot}00+04$	—	—	—	$7{\cdot}05-01$	$3{\cdot}57+00$	$3{\cdot}67+01$	$3{\cdot}86+02$	$4{\cdot}04+03$	$3{\cdot}29+04$	$1{\cdot}30+05$	$6{\cdot}17+04$	—	—	—
$3{\cdot}00+04$	—	—	$5{\cdot}13-01$	$1{\cdot}19+00$	$7{\cdot}53+00$	$8{\cdot}85+01$	$1{\cdot}11+03$	$1{\cdot}05+04$	$6{\cdot}69+04$	$1{\cdot}83+05$	$5{\cdot}16+04$	—	—	—
$2{\cdot}00+04$	—	—	$6{\cdot}12-01$	$2{\cdot}57+00$	$2{\cdot}37+01$	$2{\cdot}64+02$	$2{\cdot}52+03$	$1{\cdot}20+04$	$2{\cdot}85+04$	$4{\cdot}24+04$	$8{\cdot}03+03$	—	—	—
$1{\cdot}50+04$	—	—	$1{\cdot}08+00$	$6{\cdot}84+00$	$7{\cdot}10+01$	$5{\cdot}84+02$	$2{\cdot}15+03$	$4{\cdot}47+03$	$8{\cdot}19+03$	$1{\cdot}63+04$	$2{\cdot}96+04$	—	—	—
$1{\cdot}20+04$	—	—	$2{\cdot}20+00$	$1{\cdot}83+01$	$1{\cdot}11+02$	$3{\cdot}19+02$	$6{\cdot}10+02$	$1{\cdot}14+03$	$2{\cdot}40+03$	$5{\cdot}42+03$	—	—	—	—
$1{\cdot}00+04$	—	—	$3{\cdot}92+00$	$1{\cdot}78+01$	$3{\cdot}77+01$	$6{\cdot}61+01$	$1{\cdot}27+02$	$2{\cdot}80+02$	$7{\cdot}23+02$	$1{\cdot}76+03$	—	—	—	—
$9{\cdot}00+03$	—	$9{\cdot}12-01$	$2{\cdot}93+00$	$6{\cdot}69+00$	$1{\cdot}15+01$	$2{\cdot}19+01$	$4{\cdot}63+01$	$1{\cdot}21+02$	$3{\cdot}34+02$	—	—	—	—	—
$8{\cdot}00+03$	—	$6{\cdot}53-01$	$9{\cdot}68-01$	$1{\cdot}42+00$	$2{\cdot}57+00$	$5{\cdot}79+00$	$1{\cdot}42+01$	$4{\cdot}20+01$	$1{\cdot}34+02$	—	—	—	—	—
$7{\cdot}00+03$	—	$1{\cdot}51-01$	$1{\cdot}38-01$	$2{\cdot}13-01$	$4{\cdot}84-01$	$1{\cdot}30+00$	$3{\cdot}92+00$	$1{\cdot}33+01$	$4{\cdot}92+01$	—	—	—	—	—
$6{\cdot}00+03$	$3{\cdot}36-02$	$1{\cdot}55-02$	$1{\cdot}01-02$	$2{\cdot}21-02$	$6{\cdot}83-02$	$2{\cdot}50-01$	$1{\cdot}16+00$	$5{\cdot}31+00$	—	—	—	—	—	—
$5{\cdot}00+03$	$2{\cdot}37-03$	$1{\cdot}18-03$	$1{\cdot}30-03$	$3{\cdot}48-03$	$1{\cdot}70-02$	$1{\cdot}09-01$	$5{\cdot}17-01$	$1{\cdot}94+00$	—	—	—	—	—	—
$4{\cdot}00+03$	$1{\cdot}46-04$	$1{\cdot}47-04$	$3{\cdot}63-04$	$1{\cdot}65-03$	$7{\cdot}48-03$	$3{\cdot}10-02$	$1{\cdot}31-01$	$4{\cdot}71-01$	—	—	—	—	—	—
$3{\cdot}00+03$	$6{\cdot}51-05$	$7{\cdot}53-05$	$1{\cdot}19-04$	$2{\cdot}77-04$	$1{\cdot}08-03$	$5{\cdot}06-03$	$1{\cdot}51-02$	$3{\cdot}13-02$	—	—	—	—	—	—
$2{\cdot}50+03$	$4{\cdot}81-05$	$5{\cdot}50-05$	$8{\cdot}49-05$	$1{\cdot}62-04$	$2{\cdot}88-04$	$5{\cdot}24-04$	$1{\cdot}11-03$	$2{\cdot}19-03$	—	—	—	—	—	—
$1{\cdot}50+03$	$6{\cdot}15-06$	$5{\cdot}41-06$	$6{\cdot}26-06$	$8{\cdot}11-06$	$1{\cdot}08-05$	$1{\cdot}45-05$	$1{\cdot}96-05$	$2{\cdot}61-05$	—	—	—	—	—	—

Downloaded from https://academic.oup.com/mnras/article/144/4/485/2602797 by guest on 21 August 2022

© Royal Astronomical Society • Provided by the NASA Astrophysics Data System

1969MNRAS.144..485S

APPENDIX IV

$X = 0{\cdot}30$, $Y = 0{\cdot}64$, $Z = 0{\cdot}06$

$V(\mathrm{cm^3\ gm^{-1}})$

$T(°K)$	1·00+12	1·00+11	1·00+10	1·00+09	1·00+08	1·00+07	1·00+06	1·00+05	1·00+04	1·00+03	1·00+02	1·00+01	1·00+00	1·00−01
1·00+06	—	—	—	—	—	—	2·69−01	3·08−01	6·00−01	3·44+00	3·53+01	1·82+02	3·10+02	3·79+02
5·00+05	—	—	—	—	—	2·67−01	3·24−01	7·45−01	5·45+00	5·85+01	2·95+02	5·40+02	7·41+02	—
2·00+05	—	—	—	—	2·91−01	5·11−01	2·36+00	2·43+01	3·25+02	2·44+03	5·99+03	4·21+03	—	—
1·00+05	—	—	—	—	4·76−01	1·84+00	1·62+01	2·26+02	2·81+03	2·44+04	5·03+04	1·44+04	—	—
7·00+04	—	—	—	3·57−01	8·02−01	5·71+00	7·22+01	9·80+02	7·83+03	4·51+04	7·39+04	—	—	—
5·00+04	—	—	—	5·16−01	2·60+00	2·40+01	2·00+02	1·78+03	1·61+04	9·93+04	8·85+04	—	—	—
3·00+04	—	—	3·10−01	6·07−01	3·25+00	3·77+01	4·13+02	3·76+03	2·26+04	8·30+04	4·92+04	—	—	—
2·00+04	—	—	3·31−01	1·20+00	1·10+01	8·67+01	6·95+02	3·97+03	1·14+04	2·25+04	1·60+04	—	—	—
1·50+04	—	—	5·04−01	2·07+00	1·49+01	1·39+02	7·67+02	1·83+03	3·51+03	6·88+03	1·49+04	—	—	—
1·20+04	—	—	5·37−01	3·83+00	2·94+01	1·11+02	2·48+02	4·69+02	9·91+02	2·26+03	—	—	—	—
1·00+04	—	—	9·24−01	4·93+00	1·35+01	2·60+01	4·90+01	1·10+02	2·90+02	7·27+02	—	—	—	—
9·00+03	—	2·68−01	8·67−01	2·38+00	4·39+00	8·22+00	1·71+01	4·39+01	1·30+02	—	—	—	—	—
8·00+03	—	2·38−01	3·78−01	5·42−01	9·35−01	2·05+00	5·09+00	1·54+01	5·43+01	—	—	—	—	—
7·00+03	—	7·39−02	5·91−02	7·91−02	1·66−01	4·39−01	1·38+00	5·32+00	2·29+01	—	—	—	—	—
6·00+03	2·04−02	8·69−03	4·33−03	7·70−03	2·34−02	9·32−02	4·89−01	2·59+00	—	—	—	—	—	—
5·00+03	1·52−03	6·91−04	5·79−04	1·37−03	7·55−03	5·12−02	2·50−01	9·79−01	—	—	—	—	—	—
4·00+03	1·10−04	1·03−04	2·04−04	7·99−04	3·53−03	1·47−02	6·63−02	2·81−01	—	—	—	—	—	—
3·00+03	5·15−05	5·51−05	7·89−05	1·73−04	6·00−04	3·17−03	1·07−02	2·32−02	—	—	—	—	—	—
2·50+03	3·98−05	4·31−05	6·15−05	1·21−04	2·20−04	4·07−04	8·83−04	1·72−03	—	—	—	—	—	—
1·50+03	6·00−06	5·13−06	5·80−06	7·47−06	9·87−06	1·32−05	1·77−05	2·35−05	—	—	—	—	—	—

Downloaded from https://academic.oup.com/mnras/article/144/4/485/2602797 by guest on 21 August 2022

© Royal Astronomical Society • Provided by the NASA Astrophysics Data System